Hindawi
Advances in Civil Engineering
Volume 2020, Article ID 1853963, 14 pages
https://doi.org/10.1155/2020/1853963

Research Article

Fatigue Damage Evaluation of Pile-Supported Bridges under Stochastic Ice Loads

Tianyu Wu, Wenliang Qiu, and Guangrun Wu

School of Civil Engineering, Dalian University of Technology, No. 2 Linggong Road, Dalian City, Liaoning Province 116024, China

Correspondence should be addressed to Tianyu Wu; wty0417@mail.dlut.edu.cn and Wenliang Qiu; qwl@dlut.edu.cn

Received 9 July 2019; Revised 31 December 2019; Accepted 9 January 2020; Published 21 February 2020

Academic Editor: Constantin Chalioris

The Bohai Sea is the sea area with the worst ice condition in China, and the ice loads significantly threaten the safety of structures in the sea. The intense vibrations of the pile-supported bridge under stochastic ice loads will increase the fatigue damage of a bridge structure and reduce the fatigue life of a bridge structure. In the present study, a comprehensive analysis model is presented to study fatigue damage for pile-supported bridges under ice loads in Bohai Sea. On the basis of measured statistical data of ice parameters and stochastic ice loads spectrum of Bohai Sea, the time histories of the stochastic ice loads of Bohai Sea are simulated. Fatigue damage analysis is carried out in time domain utilizing the finite element method considering soil and bridge structure interaction. The effect of soil conditions and water depth on the cumulative fatigue damage of the pile-supported bridges is studied. Numerical results indicate that in comparison with stiff soil conditions, pile-supported bridges in soft oil conditions can increase the cumulative fatigue damage substantially; pile-supported bridges in deep water also can increase the cumulative fatigue damage obviously. The study presented the first danger position of cumulative damage of the pile cross section under stochastic ice loads. The findings of this study can be used to fatigue damage evaluation and bridge construction in the ice-covered sea area.

1. Introduction

As a natural hazard, sea ice has seriously threatened the safety of offshore structures [1–3]. The Bohai Sea is the sea area with the worst ice condition in China. There is a lot of drifting sea ice on the surface of the Bohai Sea in every winter. Ice loads occur continuously during the whole lifetime of a bridge, which will lead to excessive vibration of structures. A pile-supported bridge is the most widely used type of bridge structure in sea-crossing engineering. The stress cycles caused by ice-induced vibration can directly lead to the fatigue damage of a bridge structure. The first event of ice-induced vibration happened on the oil platform of Cook Gulf [4, 5]. After that, many vibration events were found in different frozen seas of the world [6–8]. It is notable that some offshore structures such as oil drilling platform have experienced serious ice-induced vibration events and even collapsed in the past few decades [9]. Duan et al. [10] investigated the major accident that Bohai No. 2 platform was pushed down by the sea ice in 1968 and described the whole process of platform destruction. It is pointed out that the collapse of the platform is caused by the comprehensive factors of the three aspects. The essential reason is that the fatigue damage caused by the ice-induced vibration.

The crushing failure of sea ice is the most common phenomenon in the ice failure modes when sea ice impacts on a vertical offshore structure. Yue et al. [11] carried out the field measurement on a compliant monopod platform under ice loads in Bohai Sea. The three modes of ice failure were found, and the corresponding structure vibration modes were obtained, as shown in Figure 1. The fast drifting ice is the main challenge for the offshore structures in Bohai Sea. Many researchers and engineers have made great efforts to investigate the ice loads when ice impacts on the offshore structures. Kärnä et al. [12] proposed a spectrum model of ice forces based on the field-measured data of Bohai Sea. This ice force spectrum is applied to the generation of stochastic ice loads at fast ice speed. Wu and Qiu [13] simulated the stochastic ice loads process based on ice force spectrum of Bohai Sea and verified the simulation performance. It was

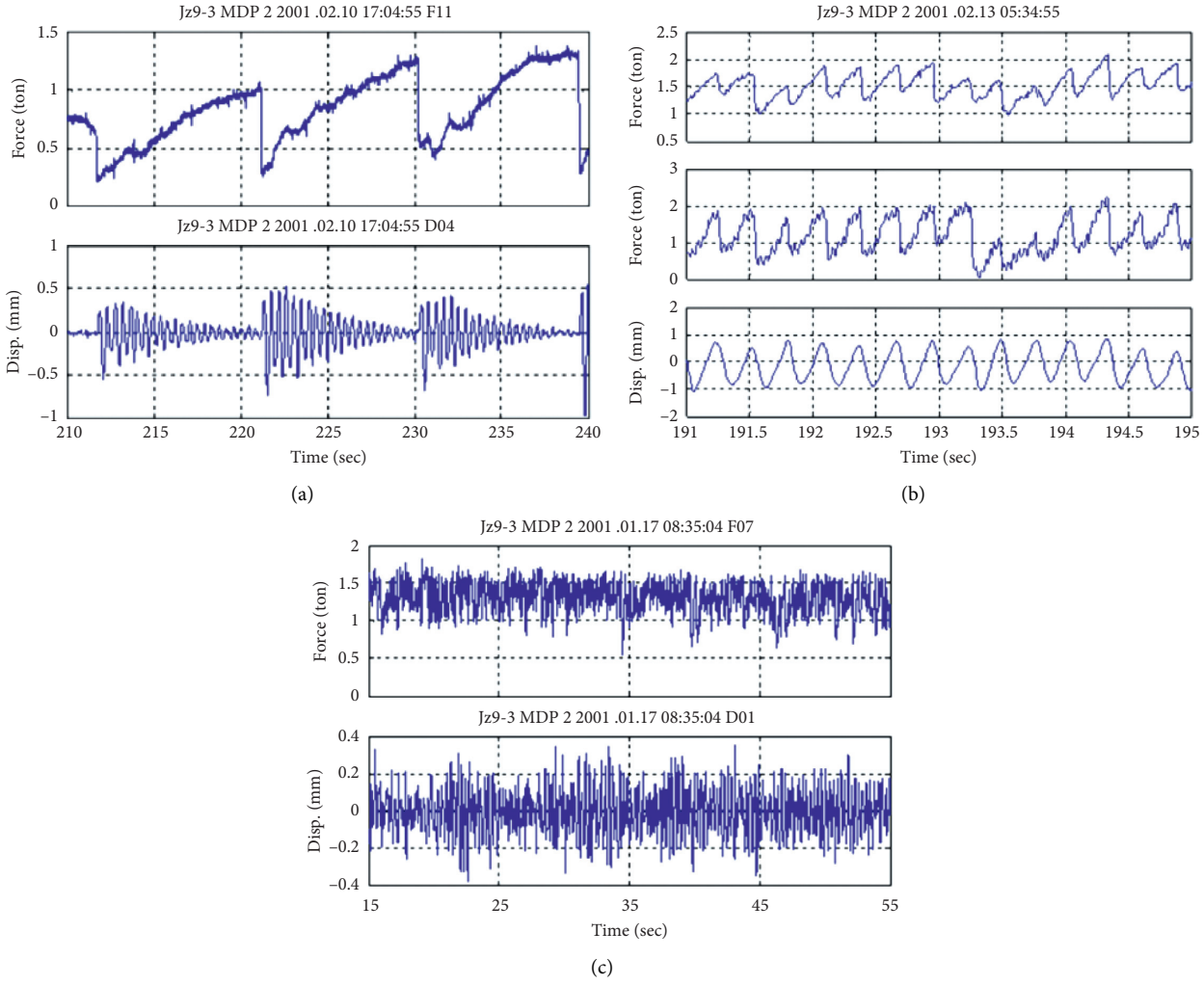

Figure 1: Ice loads and structure responses [11]. (a) Quasistatic. (b) Steady-state. (c) Stochastic.

found that the ice load spectrum model can accurately simulate the stochastic ice force of vertical structures. In the present study, the stochastic ice loads spectrum of Bohai Sea will be used to generate the stochastic ice loads process of the pile-supported bridge.

In order to maintain the safety of offshore structures, the dynamic structural characteristics should be precisely calculated under external loads. A comprehensive analysis model of a bridge structure is essential for understanding the dynamic characteristics of a structure. The pile-supported bridges are primarily constructed as a foundation type of cross-sea bridges in the deep-water region [14]. However, the soil-pile interaction can reduce the vibration frequency of the structure and even change the vibration mode of the structure, which will further affect the dynamic characteristics of the offshore structures [15]. Currently, American Petroleum Institute (API) [16] based p-y curve under cyclic load is usable to the small diameter piles, and it is the most widely used design guidelines of the offshore structures [15, 17–19]. In the present study, the p-y curves of API will be applied in the nonlinear spring of soil-pile interaction.

The fatigue damage of structural components under environmental loading is a cumulative process. Fatigue life prediction and reliability evaluation is still a challenging problem despite significant progress made in the past decades [20–25]. Sun and Jahangiri [26] studied the fatigue damage mitigation of offshore wind turbines under real wind and wave loads. The authors utilized the rain-flow cycle counting method and Miner's rule in calculating the fatigue damage. It was found that the damper of 3d-PTMD can improve the fatigue life of the offshore wind turbine effectively. Rezaei et al. [27] investigated the effect of damping on the sensitivity of the fatigue life of monopile-supported offshore wind turbines and utilized the S-N curves of DNV standard to access the fatigue damage life. This study shows that the fatigue life of the offshore structure is markedly improved due to the reduction in bending stress caused by the increased damping. Bisoi and Haldar [28] studied the effect of soil conditions on fatigue damage evaluation of offshore wind turbines. The authors considered soil-structure interaction and utilized S-N curves of DNV to access the fatigue life of offshore wind turbines. Research results show

that the fatigue life is observed to be governing design criteria for offshore wind turbines at stiff clay.

In this paper, the commercial finite element software ABAQUS is used to establish the finite element model of the offshore bridge in Bohai Sea. On the basis of measured statistical data of ice parameters and stochastic ice loads spectrum of Bohai Sea, the time histories of the stochastic ice loads of Bohai Sea are simulated. The finite element model to investigate the effects of soil conditions and water depths on the fatigue damage under stochastic ice loads is utilized. The findings of this study can be used to fatigue damage evaluation and bridge construction in the ice-covered sea area.

2. Numerical Model

2.1. Bridge Model. This paper considers a primary bridge design of the Qinhuangdao-Dalian sea-crossing bridges in Bohai Sea. The Bohai Sea is the sea area with the worst ice condition in China. There is a lot of drifting sea ice on the surface of the Bohai Sea in every winter. Figures 2 and 3 show the layout of the bridge and the main dimensions of the pier and pile sections. The sea-crossing bridges are composed of (5×120) m continuous beam with box cross section, as shown in Figure 2. The widths of the top and bottom plate are 33.1 m and 15.0 m, and the depth of the girder is 4.5 m. The shape of the pier is round-ended cross sections, and the type of the foundations is steel pipe driven pile. The pier is designed with a round-ended hollow cross section, which has a plane size of 3.5×10.0 m with a round wall thickness of 0.8 m. The size of the pile cap is $13 \times 21 \times 6$ m. 13 steel pipe piles support the pile cap with a diameter of 2.0 m, as shown in Figure 3.

The finite element model of the sea-crossing bridges is developed by utilizing the ABAQUS codes. All members of the bridge, including the main girders, piers, cap, and piles are modelled by the three-dimensional spatial beam element. The connections between the cap and piles are treated as a master-and-slave system. To consider the coupling effect between the bridge spans, three continuous girder bridges are analyzed. The total length of the simulated bridge is 1800 m which is composed of three continuous girder bridges. Each bridge has the same span arrangement of 5×120 m. In the current study, the second bridge is taken as the representative bridge, as shown in Figure 2. Structural damping was modelled by Rayleigh damping in such way that Rayleigh coefficients were determined to correspond to a 1% damping ratio at the lowest natural frequency.

2.2. Added Water Mass. When the vibration of steel pipe piles in seawater occurs, the acceleration of surrounding seawater will be affected [29]. In this study, the pile-water interaction was simulated by the additional mass method, in which the effective mass m_e of the pile can be shown as

$$m_e = m_p + m_a, \tag{1}$$

where m_p denotes the mass of pile and is the additional mass. The extra mass m_a can be expressed as

$$m_a = C_a A_p \rho_w, \tag{2}$$

where A_p is the pile cross-sectional area, $\rho_w = 1030\ \text{kg/m}^3$ denotes the density of seawater, and C_a denotes the additional mass coefficient.

The various water depths are investigated to evaluate the effect of water depths on the fatigue damage of bridges subjected to the ice loads. The water depths of $H = 10$, 20, and 30 m represent the water depths conditions of shallow, moderate, and deep water, as shown in Figure 4.

2.3. Pile-Soil Interaction. The interaction of the pile with the surrounding soil can have a significant impact on the dynamic characteristics of pile-supported bridges. To investigate fatigue damage precisely, soil-pile interaction is considered in the present study. In this study, the calculation methods of nonlinear soil spring given in API [16] and DNV [18] codes are adopted.

The *p-y* springs denote the horizontal soil resistances and the *t-z* and *Q-z* spring was set in the vertical direction to simulate the soil-pile interaction [30]. Figure 5 shows a pile foundation model with a soil spring. The API [16] and DNV [18] recommended the parameters of *p-y*, *t-z*, and *Q-z* soil spring. Nonlinear cyclic p-y curves for undrained clay ($s_u < 100$ kPa) for $Z > Z_R$ is described as

$$p = \begin{cases} 0.5 p_u \left(\frac{y}{y_c}\right)^{(1/3)}, & \text{for } y \le 3y_c, \\ 0.72 p_u, & \text{for } y \le 3y_c. \end{cases} \tag{3}$$

When $Z \le Z_R$, the *p-y* curve is described as

$$p = \begin{cases} 0.5 p_u \left(\frac{y}{y_c}\right)^{(1/3)}, & \text{for } y \le 3y_c, \\ 0.72 p_u \left\{1 - \left(1 - \left(\frac{Z}{Z_R}\right)\right) \frac{(y - 3y_c)}{12y_c}\right\}, & \text{for } 3y_c < y \le 15y_c, \\ 0.72 p_u \left(\frac{Z}{Z_R}\right), & \text{for } y > 15y_c, \end{cases} \tag{4}$$

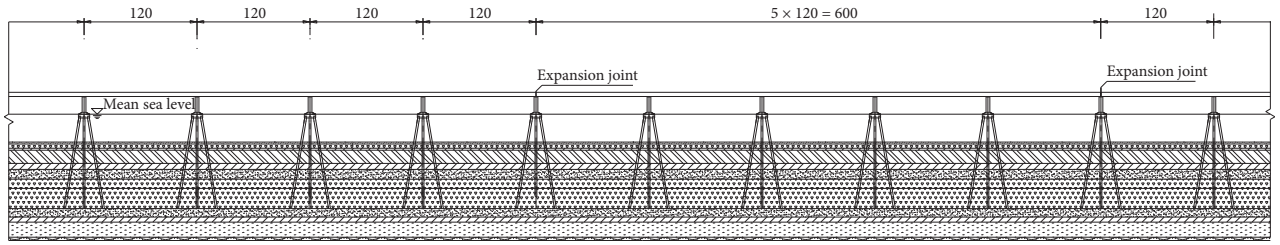

Figure 2: Configuration of the (5 × 120) m continuous bridge (unit: m).

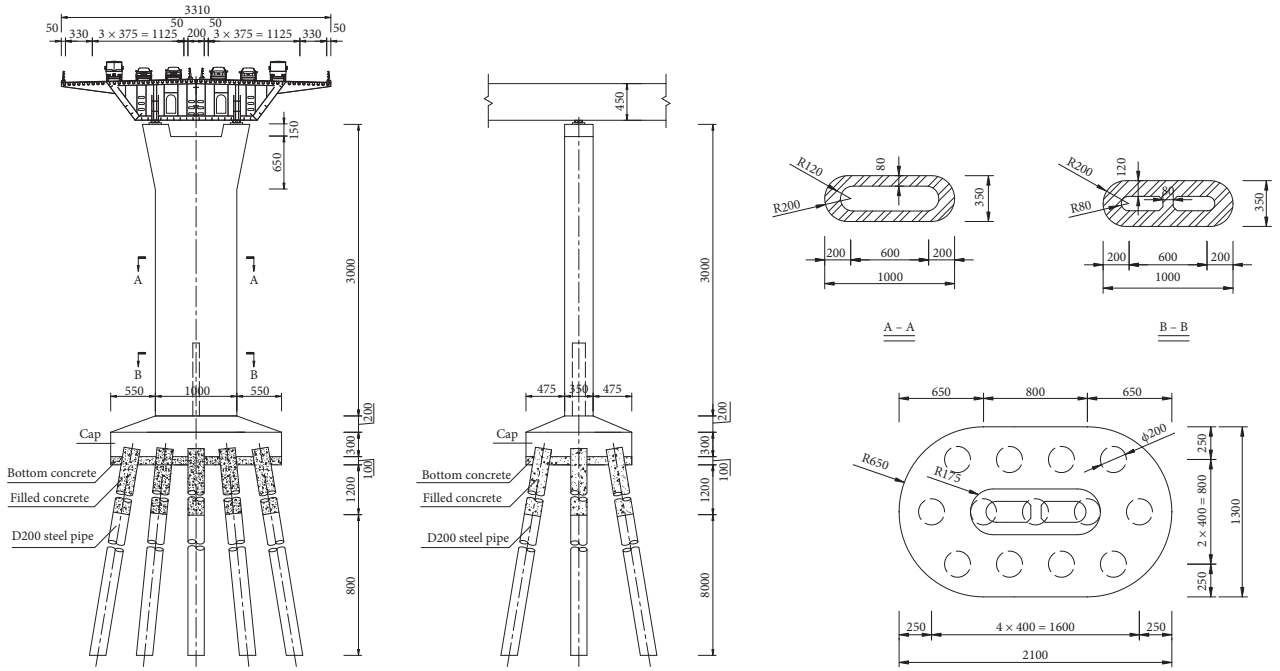

Figure 3: Configuration of bridge pier and foundation (unit: cm).

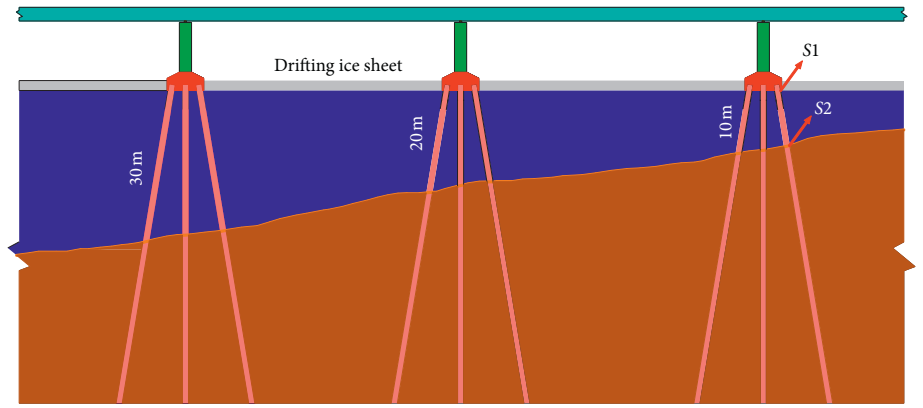

Figure 4: Exhibition of bridge configurations with 10 m, 20 m, and 30 m water depth under ice loads.

where p_u is the soil strength per unit pile length, defined as

$$p_u = \begin{cases} 3s_u + \gamma' Z + \dfrac{\mathrm{J}s_u Z}{D}, & \text{for } Z < Z_R, \\ 9s_u, & \text{for } Z \geq Z_R, \end{cases} \quad (5)$$

where γ' stand for unit weight of soil ($\gamma' = 8\,\mathrm{kN/m^3}$), s_u denotes the undrained shear strength of soil (unit: kPa), Z stands for the the below the seabed (unit: m), D denotes the pile diameter (unit: m), J represents an empirical constant ($J = 0.5$) [9], and Z_R stand for the depth below the mudline to the bottom.

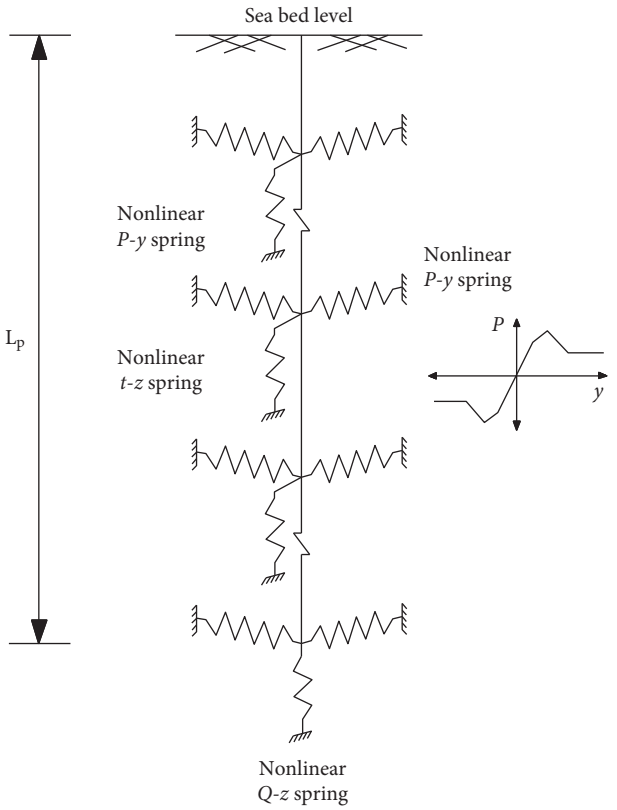

Figure 5: Schematic diagram of a soil-pile interaction model.

$$Z_R = \frac{6s_u D}{\left(\gamma' D + Js_u\right)}. \tag{6}$$

The deflection at one-half the ultimate soil resistance is estimated as

$$y_c = 2.5\varepsilon_c D, \tag{7}$$

where ε_c is the strain corresponding to one-half of the maximum stress in laboratory undrained compression tests of undisturbed soil.

The various soil conditions are investigated to evaluate the effect of soil strength on the fatigue damage of bridges subjected to the ice loads. The soil strengths of $s_u = 25$ kPa, $s_u = 50$ kPa, and $s_u = 100$ kPa represent the typical soft, moderate, and stiff soils. The corresponding values ε_c are 0.02, 0.008, and 0.006 [16]. Figure 5 shows the schematic diagram of the soil-pile interaction model and draws the lateral soil resistances (*p-y* springs), friction resistances in the vertical direction (*t-z* springs), and end bearing resistances in the vertical direction (*Q-z* springs). As an example, when soil undrained shear strengths $s_u = 25$ kPa (soft soil condition), the typical plots of nonlinear springs are drawn in Figure 6.

3. Stochastic Ice Loads Process

3.1. Probability Density of Ice Parameters in Bohai Sea. Based on the available sea ice observed data of JZ20-2 in Bohai Sea from 1996 to 2000 four winter seasons, the ice parameters of the ice thickness, ice velocity, and ice strength in the Bohai Sea were analyzed. The effective ice period in four winter seasons from 1996 to 2000 in the Bohai Sea was 44, 39, 19, and 47 days [31]. Utilizing the data samples of ice loads, the sea ice parameters were analysed statistically.

The statistical results of ice thickness h show that it obeys Log-normal distribution well. The K-S test with significant level $\alpha = 0.05$ is also passed. The distribution parameters $\mu = 1.9057$, $\sigma = 0.5732$ are obtained, and the probability density of ice thickness h can be written as [31]

$$F(h) = \frac{1}{0.5732h\sqrt{2\pi}} \exp\left[-\frac{1}{2}\left(\frac{\ln h - 1.9047}{0.5732}\right)^2\right]. \tag{8}$$

The statistical results of ice velocity v show that it obeys Rayleigh distribution well. The K-S test with significant level $\alpha = 0.05$ is also passed, and the probability density of ice velocity v can be written as [31]

$$F(v) = \frac{v}{826.5512} \exp\left(-\frac{v^2}{1653.1024}\right). \tag{9}$$

The statistical results of ice strength σ_c show that it obeys Gaussian distribution well. The K-S test with significant level $\alpha = 0.05$ is also passed. The distribution mean value $\mu = 1.0348$, the mean square error $\sigma = 0.2641$ is obtained, and the probability density of ice strength σ_c can be written as [31]

$$F(\sigma_c) = \frac{1}{0.2641\sqrt{2\pi}} \exp\left[-\frac{(\sigma_c - 1.0348)^2}{0.1395}\right]. \tag{10}$$

As described above, the ice thickness, ice velocity and ice strength can be expressed by Log-normal, Rayleigh, and Gaussian distributions. And Figure 7 shows the probability density of ice parameters (ice thickness, ice velocity, and ice strength). Due to the ice thickness, ice velocity and ice strength are relatively independent [31], the joint probability can be calculated from each two independent random variables. Figures 8(a)–8(c) show the three-dimensional data of the joint probability of ice thickness and ice velocity, ice thickness and ice strength, ice velocity and ice strength, respectively.

3.2. Spectral Model of Stochastic Ice Loads. The spectral model of ice loads was proposed by Kärnä et al. [12] based on field measurement of JZ9-3 MDP2 in Bohai Sea. The spectral model of stochastic ice loads includes auto-spectral functions and cross-spectral functions. The following is a detailed simulation process.

The auto-spectral density function of stochastic ice loads can be expressed as

$$\sigma_i^2 = \int_0^\infty G_{ii}(f)\mathrm{d}f. \tag{11}$$

The nondimensional spectrum of stochastic ice loads can be shown as

$$\widetilde{G}_{ii}(f) = \frac{fG_{ii}(f)}{\sigma_i^2}. \tag{12}$$

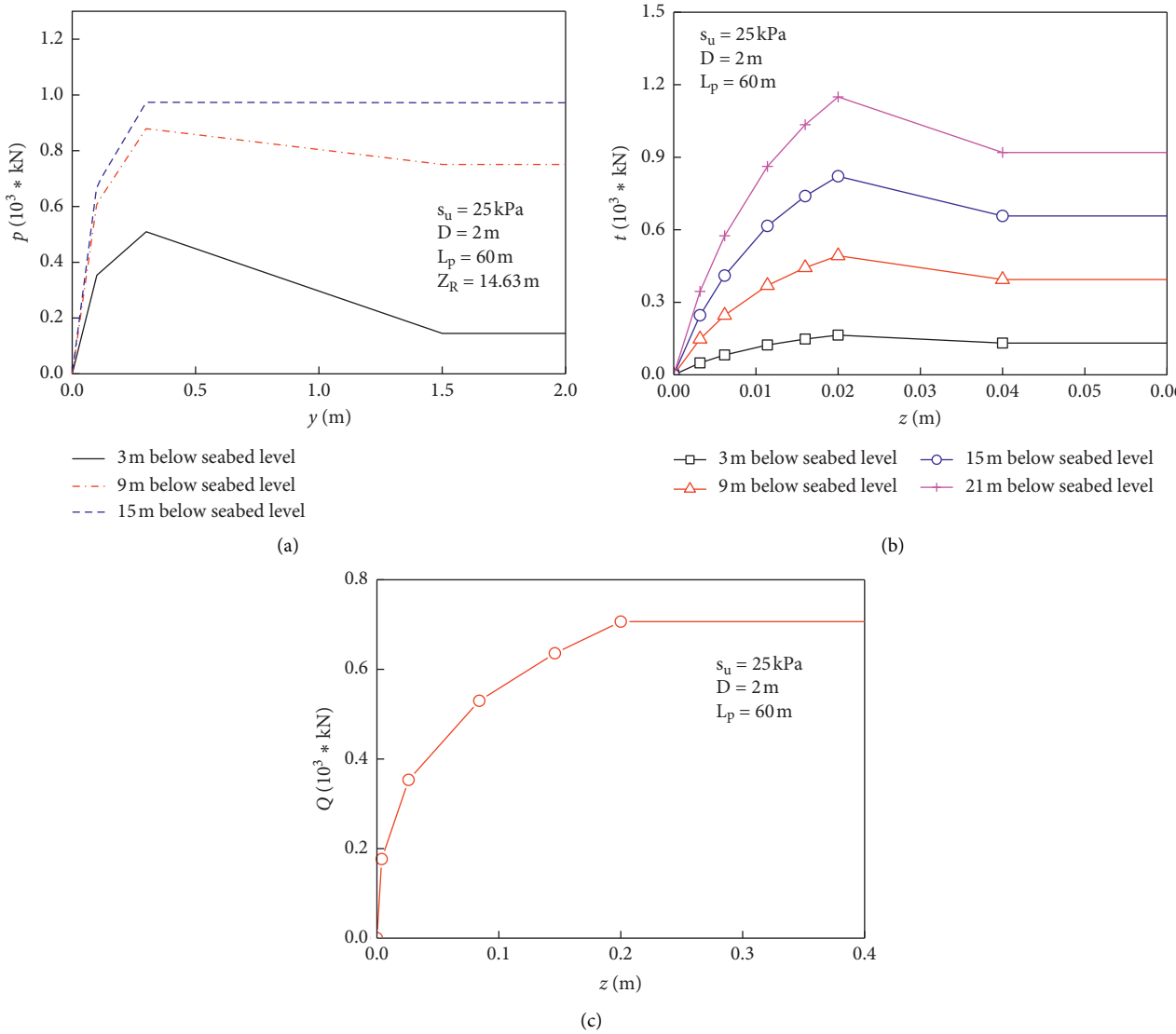

Figure 6: Typical plots of nonlinear springs: (a) p-y curve; (b) t-z curve; (c) Q-z curve.

The nondimensional auto-spectral function was proposed by Kärnä et al. [12]:

$$\widetilde{G}_{ii}(f) = \frac{af}{1 + k_s a^{1.5} f^2}, \tag{13a}$$

$$a = b \times v^{-0.6}, \tag{13b}$$

in which v stands for ice velocity and k_s and b are fitting parameters. The data analysis of stochastic ice loads in JZ9-3 MDP2 indicates that the mean value of parameter $k_s = 3.24$ and $b = 1.34$ [32].

The auto-spectral density function of local ice loads is expressed as

$$G_{ii}(f) = \frac{a}{1 + k_s a^{1.5} f^2} \sigma_i^2. \tag{14}$$

The cross-spectral density function denotes the interaction of adjacent load points i and j. The coherence function γ_{ij} is used to calculate the relations between two local points of r_{ij} distance. The coherence function γ_{ij} is expressed by auto-spectral and cross-spectral density functions as

$$\gamma_{ij}^2(f) = \frac{\left|G_{ij}(f)\right|^2}{G_{ii}(f) G_{ij}(f)}. \tag{15}$$

The coherence function was proposed by Kärnä et al. [32]:

$$\gamma_{ij} = \left(\frac{1}{1 + \rho + \alpha \xi_{ij}}\right)\left(\rho + e^{-\beta \xi_{ij} f}\right),$$
$$\xi_{ij} = \frac{r_{ij}}{h}, \tag{16}$$

in which ξ_{ij} denotes the nondimensional distance of two locations r_{ij} divided by ice thickness h. The other test parameters ρ, α, and β can be selected as $\rho = 0.1$, $\alpha = 0.2$, and $\beta = 3$ [32].

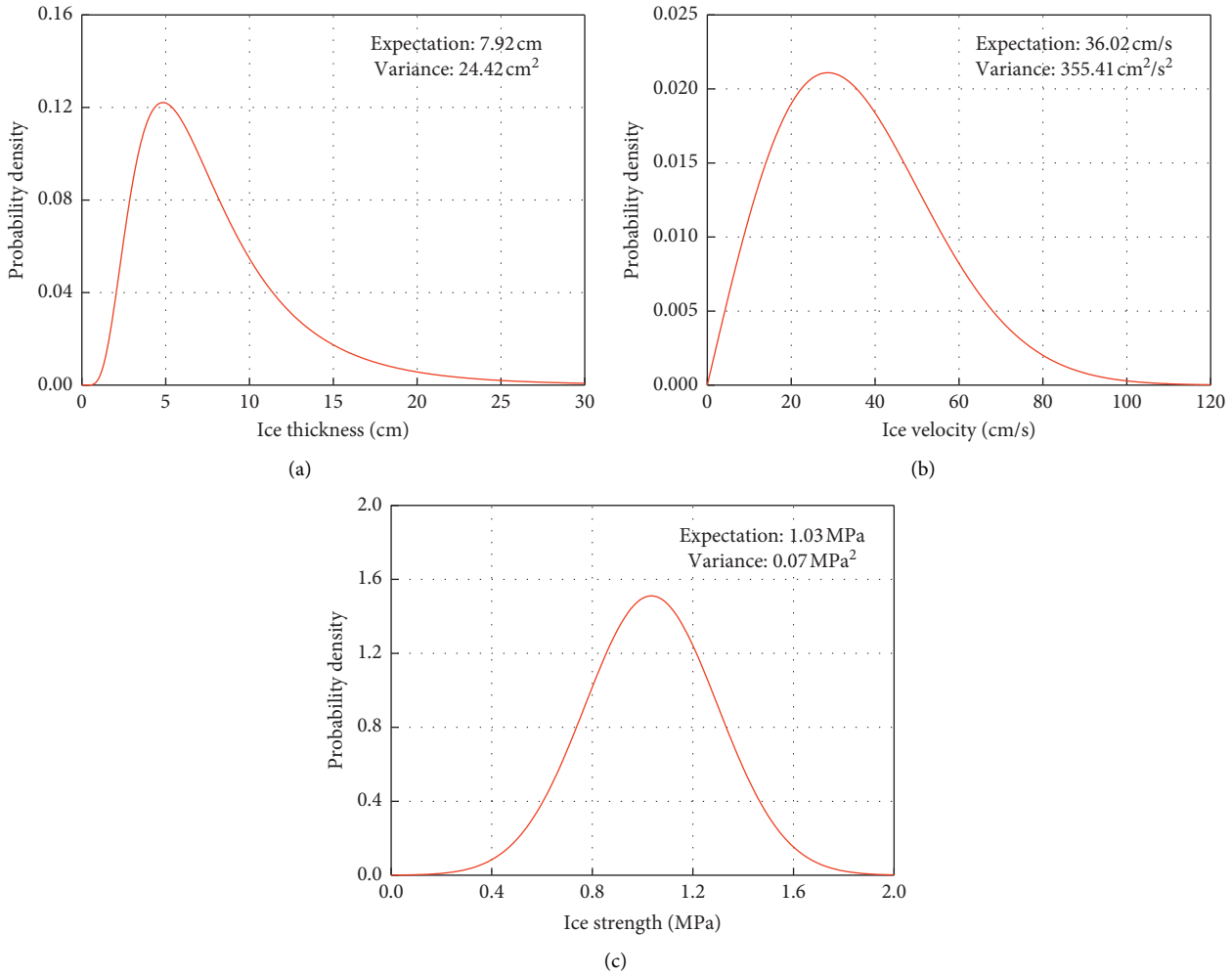

FIGURE 7: Probability density of ice parameters of JZ20-2 sea area in Bohai Sea: (a) probability density of ice thickness; (b) probability density of ice velocity; (c) probability density of ice strength.

As is shown in Figure 9, the stochastic ice loads consist of the incidence angle and shear force on the structure. The local stochastic ice loads can be expressed as

$$F_i'(t) = (\cos\theta + \mu \sin\theta) F_i(t), \tag{17}$$

where $i = 1, 2, \ldots, n$, denotes the number of parts, μ stands for the friction coefficient, and $F_i(t)$ stands for the ice loads on the contact surface.

The auto-spectral density functions of the frequency domain can be described as

$$G_{ii}'(f) = G_{ii}(f) \times \left(\cos^2\theta + \mu^2 \sin^2\theta\right). \tag{18}$$

The spectral matrices are summed to obtain the spectrum of stochastic ice loads.

$$G_F(f) = (C + \mu S)^{\mathrm{T}} G_{ff}(f)(C + \mu S), \tag{19}$$

where C and S stand for vectors for $\cos\theta$ and $\sin\theta$ at each local load point. $G_{ff}(f)$ consist of auto-spectral and cross-spectral functions.

The power spectrum of the frequency domain can be converted to the time domain.

$$F(t) = \sum \sqrt{2 \times G_F(f) \times \Delta f}\, \cos\left(2\pi f t + \varphi_f\right), \tag{20}$$

where $\sqrt{2 \times G_F(f) \times \Delta f}$ is the ice loads amplitude.

The standard deviation σ_F and mean value F_M of the time histories of ice loads can be expressed as

$$\sigma_F = \left[\int_0^\infty G_F(f)\mathrm{d}f\right]^{(1/2)}, \qquad F_M = \frac{\sigma_F}{I}. \tag{21}$$

The total ice force $F_G(t)$ against a vertical structure can be expressed as

$$F_G(t) = F_M + F(t). \tag{22}$$

Therefore, the estimation value of maximum ice loads can be expressed as

$$F_G^{\max} = F_M + k\sigma_F, \tag{23}$$

where σ_F denotes the standard deviation of stochastic ice loads and k is a selected exceedance probability. According

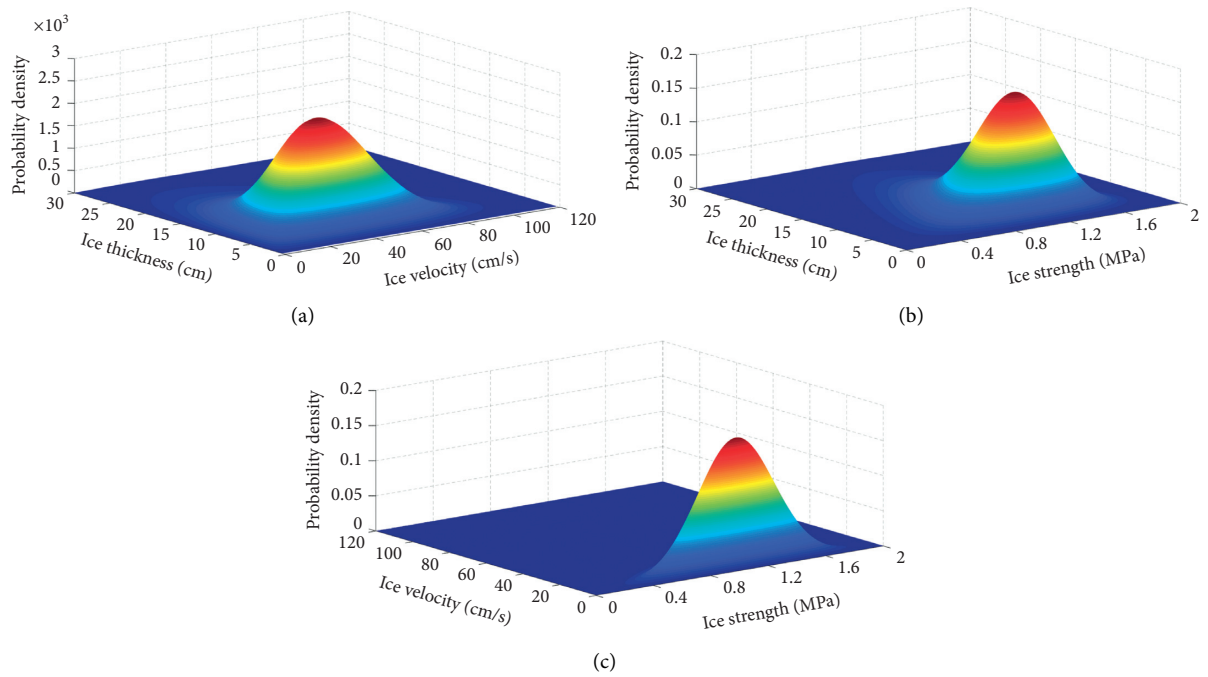

Figure 8: The joint probability density for (a) ice thickness-ice velocity; (b) ice thickness-ice strength; (c) ice velocity-ice strength.

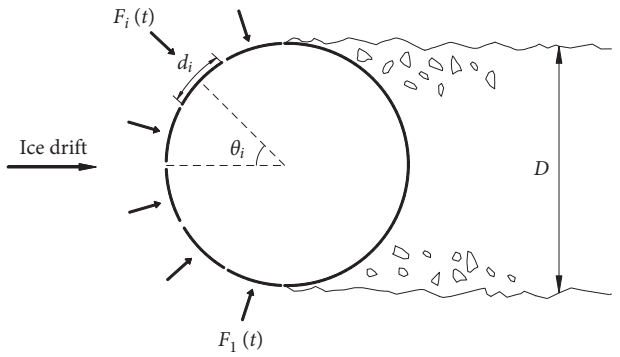

Figure 9: Ice forces distribution on an offshore structure.

to the existing references [12, 32], the assumption that the value of crushing intensity $I = 0.4$ and $k = 4.0$ is reasonable.

3.3. The Process of the Stochastic Ice Loads. The sample function of the stochastic ice loads according to the above Section 3.2 was simulated by utilizing the classical fast Fourier transforms. The upper cutoff frequency f_n was taken as 50 Hz and the total period T_0 was taken as 500 s. The ice loads time histories based on the spectral model were generated at an ice velocity of 36 cm/s, ice thickness of 8 cm, and ice strength of 1.0 MPa. For brevity, one of the ice loads time histories was displayed in this paper, as shown in Figure 10.

4. Fatigue Damage Evaluation

In this paper, the rain-flow counting methodology was utilized to evaluate the fatigue damage of the pile-supported bridge under stochastic ice loads. To investigate the fatigue damage life of the pile-supported bridge, the connection section of the piles and the cap (S_1 in Figure 4) and the piles and the seabed (S_2 in Figure 4) were calculated.

The design fatigue life of an offshore structure is determined based on the S-N curve and cumulative fatigue damage of pile-supported bridge is evaluated based on DNV [18].

$$\log_{10}^{N} = \log_{10}^{a} - m \log_{10}\left(\Delta\sigma\left(\frac{t}{t_{\text{ref}}}\right)^{k}\right), \tag{24}$$

where N denotes the predicted fatigue damage in cycles; $\Delta\sigma$ denotes the stress range; m denotes the negative slope of S-N curve; $\log^{a}$ is the intercept of $\log^{N}$ axis; t is plate thickness; t_{ref} is the reference thickness and k denotes the thickness exponent.

According to DNV standard, the S-N curve parameters for a pile are shown in Table 1. After rain-flow counting for each stress range $\Delta\sigma$ is processed, Miner's sum can calculate a cumulative fatigue damage:

$$D_j = \sum_{i=1}^{I} \frac{n_i}{N_i}, \tag{25}$$

in which n_i denotes the number of stress cycles in a given stress block, and N_i stands for the number of stress cycles to fatigue failure in a given stress block.

The total cumulative fatigue damage is calculated as follows:

$$D = \sum_{j=1}^{64} P_j D_j, \tag{26}$$

where P_j is the probability value of each ice load case. D_j is the fatigue damage value of each ice load case.

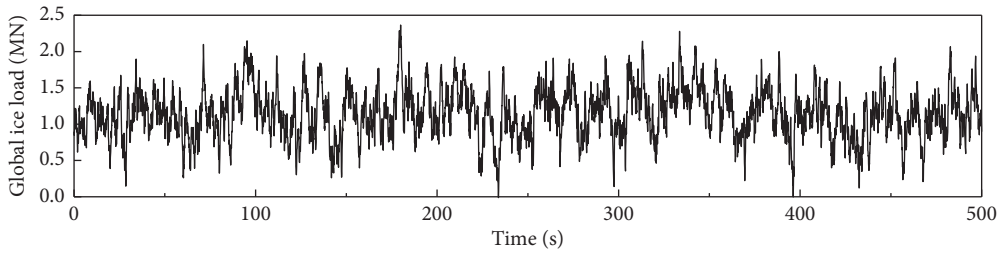

Figure 10: The time history of the stochastic ice force for the present bridge ($T = 500$ s).

Table 1: S-N curves parameters, according to [18].

$N \le 10^6$		$N \ge 10^6$		Fatigue limit at 10^7 cycles	Thickness ratio	Thickness component	Stress concentration factor
$\text{Log}(a_1)$	m_1	$\text{Log}(a_2)$	m_2	σ (MPa)	t/t_{ref}	k	SCF
11.61	3.0	15.35	5.0	46.78	1.0	0.2	1.13

Fatigue damage evaluation was applied by utilizing stochastic ice loads histories. The fatigue damage at the pile top and seabed cross section was evaluated by utilizing the rain-flow counting methodology. Figures 7(a)–7(c) show a dominant range of ice parameters: ice thickness below 20 cm, ice velocity below 80 cm/s, and ice strength below 1.6 MPa, respectively. The joint probability of ice thickness, ice velocity, and ice strength are determined for the ice thickness range from 3 to 20 cm, the ice velocity range from 10 to 80 cm/s, and the ice strength range from 0.4 to 1.6 MPa. To reduce the computational cost, the ice thickness, ice velocity, and ice strength are divided into 4 bins, respectively. 64 ice loads cases are selected in this paper. Ice thickness is chosen as 4 cm, 8 cm, 12 cm, and 16 cm. The ice velocity values are selected as 16 cm/s, 36 cm/s, 56 cm/s, and 76 cm/s. Four representative ice strengths are used: 0.5 MPa, 1.0 MPa, 1.5 MPa, and 2.0 MPa.

Considering that sea ice impact on the pile cap of the pile-supported bridge and largest total stress is expected to be at pile top cross section or seabed cross section. The selected bending stress points are shown in Figure 11. The overall bending stress of the selected stress point can be expressed as

$$\sigma_i = \frac{N}{A} + \frac{M_y}{I_y} r \cos \varphi_i, \tag{27}$$

in which N denotes the axial force and A stand for the section area, r denotes the section radius, M_y stands for the bending moments, and I_y denotes the moments of cross-section area.

5. Results

Various soil conditions are investigated to evaluate the effect of soil strength on the fatigue damage of bridges subjected to the ice loads. The soil strengths of $s_u = 25$ kPa, $s_u = 50$ kPa, and $s_u = 100$ kPa represent the typical soft, moderate, and stiff soils. Based on the determined number of stress cycles and stress ranges, the fatigue damage is evaluated based on the S-N curve and Miner's rule.

The total cumulative damage of the five selected points is evaluated by utilizing the rain-flow cycle counting

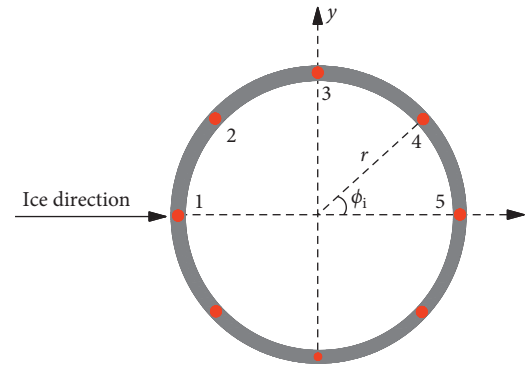

Figure 11: Selected stress points distributed along the pile cross section.

methodology to calculate the stress cycles of a pile-supported bridge under each ice load case. In this paper, the effect of soil strength conditions and water depth on the fatigue damage of a bridge structure is investigated systematically. The selected stress point is investigated by utilizing equation (27) within 500 s to reduce the computational cost. For fatigue damage estimation, the response of the structure is calculated for all selected ice parameters. Due to the limitation of paper length, the response of the structure corresponding to ice velocity $v = 36$ cm/s, ice thickness $h = 8$ cm, and ice strength $\sigma = 1.0$ MPa, are shown as an example in Figures 12–15.

Figures 12 and 13 show the bending stress time histories for different soil conditions at S_1 and S_5 on the pile top and seabed cross section, respectively. Table 2 tabulates the cumulative fatigue damage results of the selected 5 locations at the pile top and seabed cross section with a different undrained shear strength of the soil. It can be found that S_{1i} denotes the selected points distributed along the pile top cross section and S_{2i} denotes the selected points distributed along the seabed cross section.

As shown in Figures 12 and 13, the range of stress amplitude of pile top cross section are higher than seabed cross section. This phenomenon is due to the sea ice impact on the pile cap directly, which leads to higher

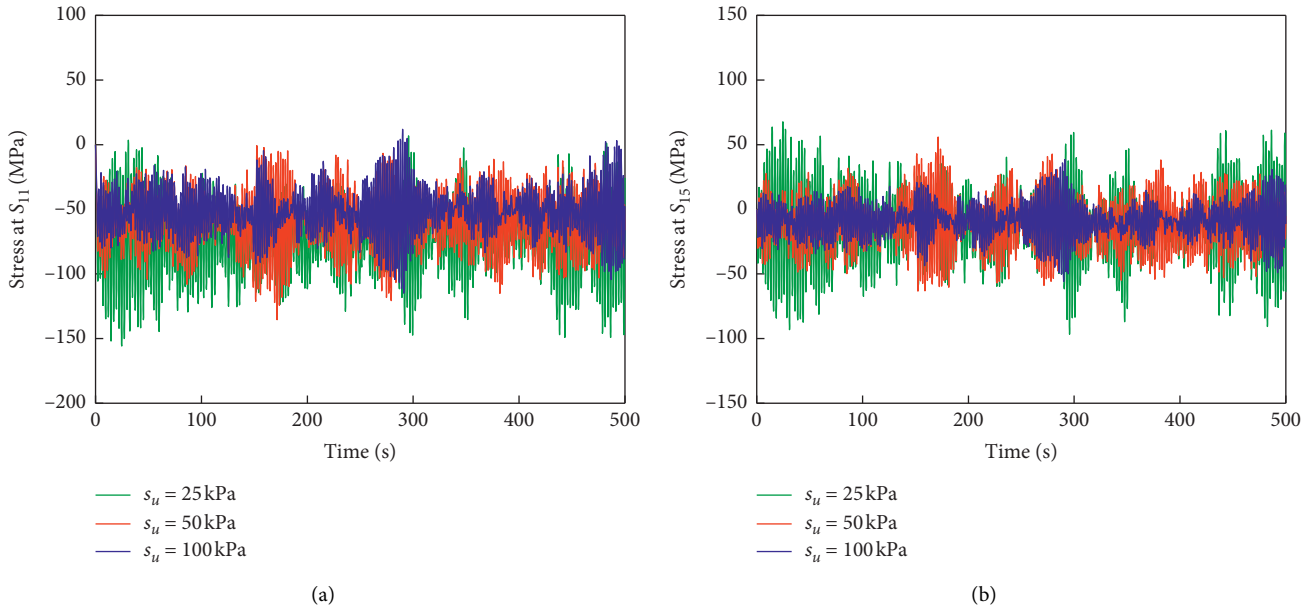

FIGURE 12: Comparison of stress at the pile top cross section for different soil conditions: (a) time histories of stress at S_{11}; (b) time histories of stress at S_{15} ($v = 36$ cm/s, $h = 8$ cm, $\sigma = 1.0$ MPa).

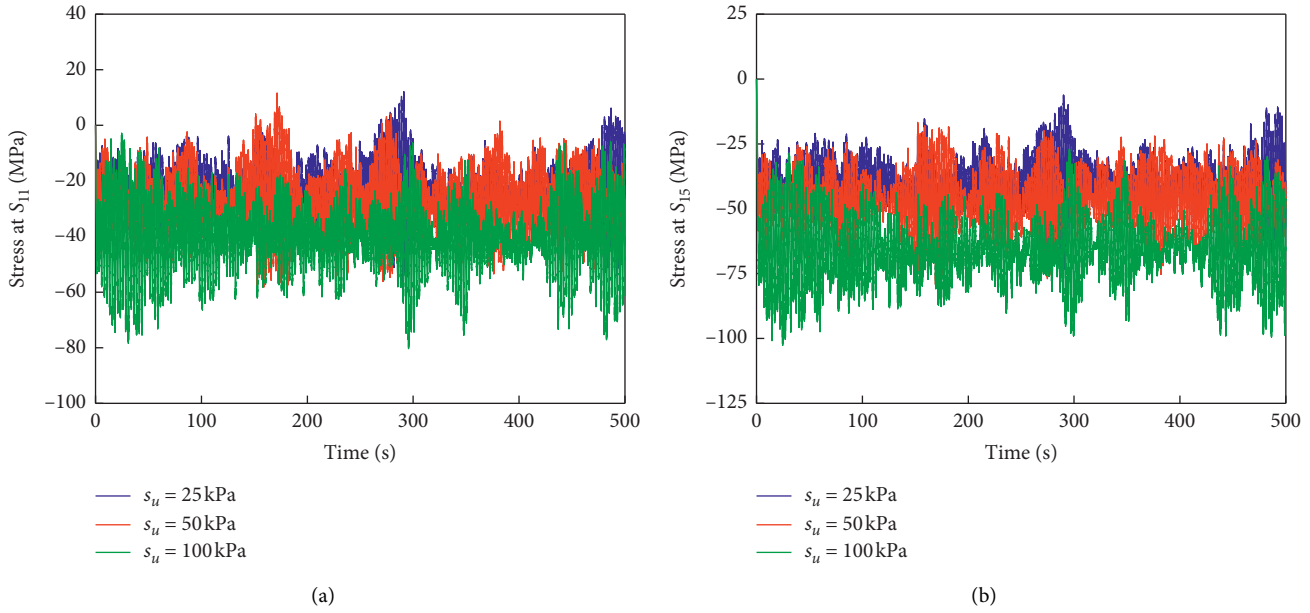

FIGURE 13: Comparison of stress on seabed cross section for different soil conditions: (a) time histories of stress at S_{11}; (b) time histories of stress at S_{15} ($v = 36$ cm/s, $h = 8$ cm, $\sigma = 1.0$ MPa).

stress cycles than the latter. Due to the increase of undrained shear strength, the lateral stiffness of soil increases, which leads to the decrease of stress amplitude range of pile and seabed significantly. This phenomenon is a reason that the piles insert into the seabed and is surrounded by the different stiffness of soil, which makes the pile-supported bridge dissipates less energy compared with the stiff soil. As shown in Figure 12(a) and Table 2, the cumulative fatigue damage at S_{11} of the pile top cross section are $2.492e^{-4}$ and $1.353e^{-4}$, respectively, when $s_u = 25$ and 50 kPa, which increase by 222.3% and 75.0% compared to soil strength $s_u = 100$ kPa. Figure 13(a) and Table 2 also show that when soil strength $s_u = 25$ and 50 kPa, cumulative fatigue damage at S_{21} of the seabed cross section are $0.157e^{-4}$ and $0.111e^{-4}$. The results of the cumulative fatigue damage increased by 282.9% and 170.7%, respectively, compared to the case of stiff soil condition. It is notable that the different soil conditions should be considered to more accurately predict the fatigue damage of the pile-supported bridge.

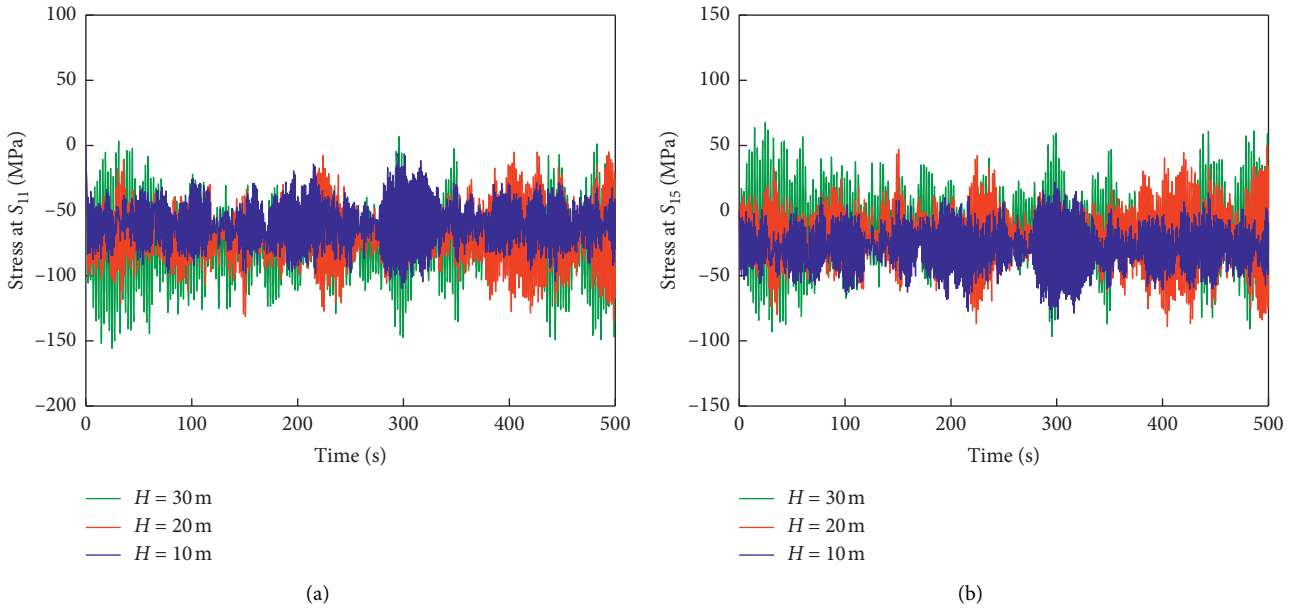

FIGURE 14: Comparison of stress at the pile top cross section with different water depth: (a) time histories of stress at S_{11}; (b) time histories of stress at S_{15} ($v = 36$ cm/s, $h = 8$ cm, $\sigma = 1.0$ MPa).

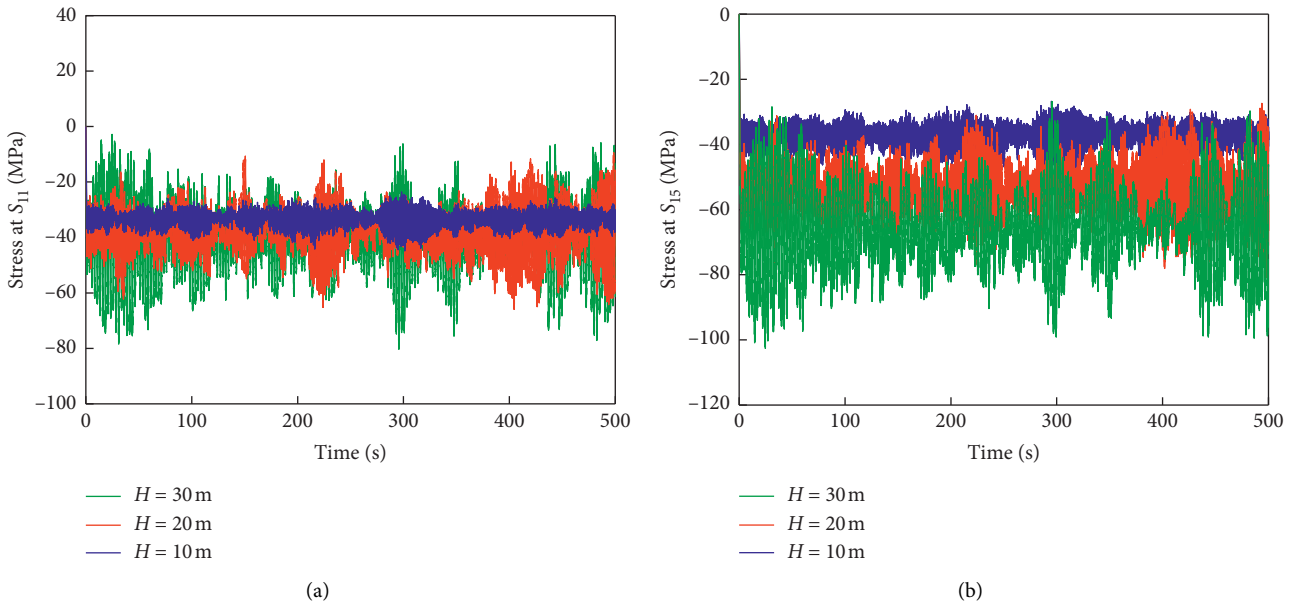

FIGURE 15: Comparison of stress on seabed cross section with different water depth: (a) time histories of stress at S_{11}; (b) time histories of stress at S_{15} ($v = 36$ cm/s, $h = 8$ cm, $\sigma = 1.0$ MPa).

The various water depths are investigated to evaluate the effect of water depths on the fatigue damage of bridges subjected to the ice loads. The water depths of $H = 10$, 20, and 30 m represent the water depths conditions of shallow, moderate, and deep water.

Figures 14 and 15 show the bending stress time histories for different water depths at S_1 and S_5 on the pile top and seabed cross section, respectively. Table 3 tabulates the cumulative fatigue damage results of the selected 5 locations at the pile top and seabed cross section with different water depths. According to equation (27), we can see that the total bending stress of selected stress points can be influenced by bending moments, and the distance between the neutral axis and stress points. Consequently, the fluctuation of stress amplitude decreases from stress point S_{11} to S_{13} and then increases from stress point S_{13} to S_{15}. Larger stress amplitudes can result in greater fatigue damage. As tabulated in Table 3, the cumulative fatigue damage of stress points of ice impact direction is more than that of any other positions of the pile cross section. Due to the direct effect of ice impact

Table 2: 500 s cumulative fatigue damage with different soil conditions (water depth: 30 m).

Position	Position along pile section	Cumulative damage (10^{-4})		
		$S_u = 25$ kPa (soft)	$S_u = 50$ kPa (medium)	$S_u = 100$ kPa (stiff)
Pile-top	S_{11}	2.492	1.353	0.773
	S_{12}	1.604	0.937	0.354
	S_{13}	0.101	0.054	0.021
	S_{14}	1.479	0.793	0.216
	S_{15}	2.221	0.962	0.614
Seabed	S_{21}	0.157	0.111	0.041
	S_{22}	0.095	0.068	0.017
	S_{23}	0.007	0.003	0.001
	S_{24}	0.079	0.052	0.011
	S_{25}	0.132	0.102	0.034

Table 3: 500 s cumulative fatigue damage with different water depths (soil strength: 25 kPa).

Position	Position along pile section	Cumulative damage (10^{-4})		
		$H = 30$ m (deep)	$H = 20$ m (medium)	$H = 10$ m (shallow)
Pile-top	S_{11}	2.492	1.659	0.863
	S_{12}	1.604	1.055	0.475
	S_{13}	0.101	0.084	0.044
	S_{14}	1.479	0.993	0.389
	S_{15}	2.421	1.426	0.822
Seabed	S_{21}	0.157	0.122	0.049
	S_{22}	0.095	0.078	0.028
	S_{23}	0.007	0.004	0.002
	S_{24}	0.079	0.066	0.019
	S_{25}	0.132	0.093	0.026

direction, the larger bending stress amplitude happened at stress points S_{11} and S_{15}. However, the bending stress of the stress point S_{13} is minimum. This reason is the stress point S_{13} is perpendicular and far away from the action direction of ice loads, i.e., stress point S_{13} is on the neutral axis. The numerical result indicates that the cumulative fatigue damage decreases from stress point S_{11} to S_{13} and then increases from stress point S_{13} to S_{15}. The variation tendency of the cumulative fatigue damage of stress points along the pile section was similar on the seabed cross section. As shown in Figures 14 and 15, the stress amplitude range of the pile top cross section is much larger than seabed cross section. This phenomenon is due to the cross section of the pile top experiences higher stress amplitudes than the cross section of the seabed when sea ice impacts on the pile cap directly.

The range of the stress amplitude of the pile top and seabed cross sections increases with the water depth. As shown in Figure 14(a) and Table 3, when the water depth is 30 m and 20 m, the cumulative fatigue damage at S_{11} of the pile top cross section are $2.492e^{-4}$ and $1.659e^{-4}$. The corresponding results are 188.7% and 92.2% higher than that of water depth of 10 m. Figure 15(a) and Table 3 also show that when the water depth is 30 and 20 m, the cumulative fatigue damage at S_{21} of the seabed cross section is $0.157e^{-4}$ and $0.122e^{-4}$. The results of the cumulative fatigue damage increased by 220.4% and 148.9%, respectively, compared to the case of shallow water depths. Note that the effect of water depth on the fatigue damage of the pile-supported bridge is essential and the different water depth should be considered to predict the fatigue damage reasonably.

6. Conclusions

A pile-supported bridge is the most widely used type of bridge structure in sea-crossing engineering. The stress cycles caused by ice-induced vibration can directly lead to the fatigue damage of the bridge structures. In this paper, the fatigue damage of the pile-supported bridge was analyzed based on the bending stress induced by the bridge vibrations under ice loads. The effects of soil conditions and water depths on the fatigue damage of the pile-supported bridge were investigated by utilizing the rain-flow counting method.

The statistical data of the ice parameters of Bohai Sea including the ice thickness, ice velocity, and ice strength are investigated. The statistical ice parameters of Bohai Sea are essential for evaluating fatigue damage of pile-supported bridges in this paper and are greatly significant for the construction project of the pile-supported bridges in Bohai Sea.

By calculating the fatigue damage caused by the ice load of each bin and considering its probability, the total fatigue damage within 500 s is calculated. The results show that the cumulative fatigue damage of piles with soft soil condition is much larger than those with stiff soil condition and that the deep-water condition also can increase the fatigue damage markedly. Furthermore, it can be seen that the whole

bending stress of selected stress points can be influenced by bending moments and the distance between the neutral axis and stress points. The larger stress amplitudes can result in greater fatigue damage. The cumulative fatigue damage of stress points of ice impact direction is higher than any other position of the pile cross section. The stress amplitude range of the pile top cross section is much larger than the seabed cross section. This phenomenon is due to the cross section of the pile top experiences higher stress amplitudes than the cross section of the seabed when sea ice impacts on the pile cap directly. This provides significant design guidance for the construction and evaluation of the pile-supported bridge in the ice-covered sea area.

Data Availability

The data used to support the findings of this study are available from the corresponding author upon request.

Conflicts of Interest

The authors declare that they have no conflicts of interest.

Acknowledgments

This study was funded by the National Natural Science Foundation of China (grant number: 51778108).

References

[1] R. Frederking and D. Sudom, "Maximum ice force on the Molikpaq during the April 12, 1986 event," *Cold Regions Science and Technology*, vol. 46, no. 3, pp. 147–166, 2006.

[2] T. G. Brown, "Analysis of ice event loads derived from structural response," *Cold Regions Science and Technology*, vol. 47, no. 3, pp. 224–232, 2007.

[3] Q. Yue, Y. Qu, X. Bi, and K. Tuomo, "Ice force spectrum on narrow conical structures," *Cold Regions Science and Technology*, vol. 49, no. 2, pp. 161–169, 2007.

[4] H. R. Peyton, "Sea ice forces. Ice pressures against structures," *Technical Memorandum*, vol. 92, pp. 117–123, 1968.

[5] K. A. Blenkarn, "Measurement and analysis of ice forces on Cook Inlet structures," in *Proceedings of the Offshore Technology Conference*, Houston, TX, USA, April 1970.

[6] A. Engelbrektson, "Dynamic ice loads on a lighthouse," in *Proceedings of the Port and Ocean Engineering Under Arctic Conditions*, pp. 654–663, Helsinki, Finland, 1977.

[7] D. S. Sodhi, "Ice-induced vibrations of structures," in *Proceedings of the Ninth International Association of Hydraulic Engineering and Research Symposium on Ice*, pp. 625–657, Yokohama, Japan, August 1988.

[8] Q. Yue, X. Zhang, X. Bi, and Z. Shi, "Measurements and analysis of ice induced steady state vibration," in *Proceedings of the International Conference on Port and Ocean Engineering under Arctic Conditions*, Ottawa , Canada, 2001.

[9] H. Fang, M. Duan, and F. Xu, "Reliability analysis of ice-induced fatigue and damage in offshore engineering structures," *China Ocean Engineering*, vol. 14, no. 1, pp. 15–24, 2000.

[10] M. Duan, H. Fang, and R. Chen, "The investigation conclusion of Bohai Lao 2 platform being pushed down by ice," *Oil Field Equipment*, vol. 23, no. 3, pp. 1–4, 1994.

[11] Q. Yue, F. Guo, and T. Kärnä, "Dynamic ice forces of slender vertical structures due to ice crushing," *Cold Regions Science and Technology*, vol. 56, no. 2-3, pp. 77–83, 2009.

[12] T. Kärnä, Y. Qu, X. Bi, Q. Yue, and W. Kuehnlein, "A spectral model for forces due to ice crushing," *Journal of Offshore Mechanics and Arctic Engineering*, vol. 129, no. 2, pp. 138–145, 2007.

[13] T. Wu and W. Qiu, "Simulation of stochastic ice force process of vertical offshore structure based on spectral model," *Computer Modeling in Engineering & Sciences*, vol. 115, no. 1, pp. 47–66, 2018.

[14] G. M. Álamo, J. J. Aznárez, L. A. Padrón, A. E. Martínez-Castro, R. Gallego, and O. Maeso, "Dynamic soil-structure interaction in offshore wind turbines on monopiles in layered seabed based on real data," *Ocean Engineering*, vol. 156, pp. 14–24, 2018.

[15] Y. E. Mostafa and M. H. El Naggar, "Response of fixed offshore platforms to wave and current loading including soil-structure interaction," *Soil Dynamics and Earthquake Engineering*, vol. 24, no. 4, pp. 357–368, 2004.

[16] American Petroleum Institute (API), *Petroleum and Natural Gas Industries-specific Requirements for Offshore Structures. Part 4-geotechnical and Foundation Design Considerations*, American Petroleum Institute (API), Washington, DC, USA, 2011.

[17] L. V. Andersen, M. J. Vahdatirad, M. T. Sichani, and J. D. Sørensen, "Natural frequencies of wind turbines on monopile foundations in clayey soils-A probabilistic approach," *Computers and Geotechnics*, vol. 43, pp. 1–11, 2012.

[18] DNV-OS-J101, *Design of Offshore Wind Turbine Structures*, Det Norske Veritas, Oslo, Norway, 2010.

[19] Germanischer Lloyd (GL), *Guideline for the Certification of Offshore Wind Turbines*, Germanischer Lloyd (GL), Hamburg, Germany, 2005.

[20] J. Du, H. Li, M. Zhang, and S. Wang, "A novel hybrid frequency-time domain method for the fatigue damage assessment of offshore structures," *Ocean Engineering*, vol. 98, pp. 57–65, 2015.

[21] W. Huang, "The frequency domain estimate of fatigue damage of combined load effects based on the rain-flow counting," *Marine Structures*, vol. 52, pp. 34–49, 2017.

[22] D. Zwick and M. Muskulus, "Simplified fatigue load assessment in offshore wind turbine structural analysis," *Wind Energy*, vol. 19, no. 2, pp. 265–278, 2016.

[23] S. F. Mohammadi, N. S. Galgoul, U. Starossek, and P. M. Videiro, "An efficient time domain fatigue analysis and its comparison to spectral fatigue assessment for an offshore jacket structure," *Marine Structures*, vol. 49, pp. 97–115, 2016.

[24] B. Yeter, Y. Garbatov, and C. Guedes Soares, "Evaluation of fatigue damage model predictions for fixed offshore wind turbine support structures," *International Journal of Fatigue*, vol. 87, pp. 71–80, 2016.

[25] B. Yeter, Y. Garbatov, and C. Guedes Soares, "Fatigue damage assessment of fixed offshore wind turbine tripod support structures," *Engineering Structures*, vol. 101, pp. 518–528, 2015.

[26] C. Sun and V. Jahangiri, "Fatigue damage mitigation of offshore wind turbines under real wind and wave conditions," *Engineering Structures*, vol. 178, pp. 472–483, 2019.

[27] R. Rezaei, P. Fromme, and P. Duffour, "Fatigue life sensitivity of monopile-supported offshore wind turbines to damping," *Renewable Energy*, vol. 123, pp. 450–459, 2018.

[28] S. Bisoi and S. Haldar, "Design of monopile supported offshore wind turbine in clay considering dynamic soil-

structure-interaction," *Soil Dynamics and Earthquake Engineering*, vol. 73, pp. 103–117, 2015.

[29] C.-Y. Liaw and A. K. Chopra, "Dynamics of towers surrounded by water," *Earthquake Engineering & Structural Dynamics*, vol. 3, no. 1, pp. 33–49, 1974.

[30] H. Zuo, K. Bi, and H. Hao, "Dynamic analyses of operating offshore wind turbines including soil-structure interaction," *Engineering Structures*, vol. 157, pp. 42–62, 2018.

[31] X. Ji, Q. Yue, and X. Bi, "Probability distribution of sea ice fatigue parameters in JZ20-2 sea area of the Liaodong Bay," *The Ocean Engineering*, vol. 20, no. 3, pp. 39–43, 2002.

[32] T. Karna, Y. Qu, and W. L. Kühnlein, "A new spectral method for modeling dynamic ice actions," in *Proceedings of the ASME 2004 23rd International Conference on Offshore Mechanics and Arctic Engineering*, pp. 953–960, Vancouver, Canada, June 2004.